

M98-D3: High Stress Elastic Materials

Team: Julie Chen (leader), University of Massachusetts - Lowell
Robert A. DaSilva, Graduate Student, Univ of Massachusetts – Lowell
Steve Warner, University of Massachusetts – Dartmouth
Armand Lewis, University of Massachusetts- Dartmouth

Goals: The primary objective of this project is the development of a generalized model for linear textile structures. Longer term goals within the project scope include further investigation of the development of novel structures achieved through hybridization and parameter modification of traditional textiles. The aim is to produce braids with anomalously high levels of toughness.

ABSTRACT

This paper addresses the phenomenology of strand interaction in biaxial non-embedded braided textile structures under uniaxial tension. The specific interest in the development of new braided textile structures is a result of the shortcomings of current rope, belt, and cable performance under large strain controlled conditions. In this paper, a generalized model is developed for these structures with the intent of characterizing and predicting mechanical behavior. The methodology consists of a modular framework, which includes the prediction of manufacturing parameters. Lateral strand compaction tests were performed to generate constitutive material curves for use in analytical geometric models. Model predictions correlate well with data generated from braid uniaxial tension tests. Results suggest that lateral strand strain drives braid tensile behavior.

KEY WORDS: Braid Model, Fiber Compaction, Composite Preform, Rope, Mooring Line

INTRODUCTION

The work presented in this paper, and the interest in the development of new braided textile structures is a result of the shortcomings of current rope, belt, and cable performance under large strain controlled conditions. Examples of this characteristic problem can be found in innumerable places, but is particularly problematic in oceanic mooring applications such as the tethering of oil rig platforms. The typically high modulus lines exhibit desirably “stiff” behavior under normal conditions to control buoyant rigid body modes and drifting. However, under storm conditions, they are unable to comply with the necessary elongation needed to absorb high amplitude wave energy [1]. Often times, failure of a tension member is disastrous and causes listing and eventual capsizing of the vessel or rig.

This problem is prevalent in braided rope structures, because it is inherent to the nature of the deformation mechanism at each structural level of the rope [2,3]. That is, deformation characteristics from the fiber compaction level to the rope extension level, all share the same trend of increasing in stiffness with increasing strain in the elastic strain region. The traditional braided structure response under uniaxial tension is characterized by three distinct regimes in the

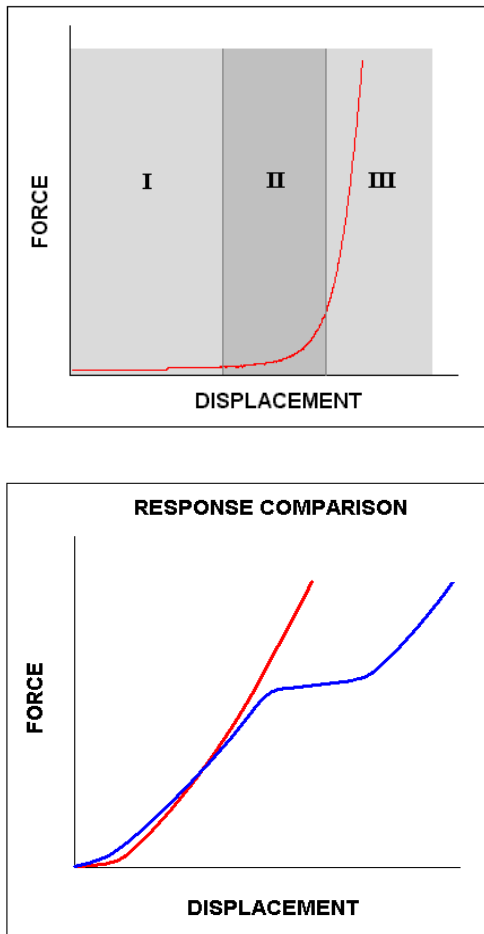


Fig. 1. Typical (red) and Novel (blue) force vs. displacement curves for braided structures.

decreased stiffness (increased strain) under extreme conditions without incurring significant damage (Fig. 1).

To study this concept further, compaction tests were performed on strands comprised of hollow fibers. Figure 2 compares the results from the tests with solid fibers of the same material. As can be seen, there exists a slight knee in the hollow fiber curve that occurs around 6 KN. Although minor in this particular case, this example suggests that a structure could be designed to exhibit the desired novel response shown in Fig. 1. The applications of this mechanism include not only improved mooring lines, but also the possibility of braided preforms with reduced wrinkling and increased formability. Thus, the goal of this work is to develop a simple, but accurate model for the response of these braided structures. This model can be used to predict the proper percentage and properties of hollow fibers needed to obtain the desired plateau behavior.

force vs. displacement curve; namely, I.) flattened or zero load, II.) ramped, and III.) stiffened (Fig. 1).

Each of these regions is representative of a state of fabric shear deformation. In the first region, spacing between the adjacent strands or gaps between the sheath and core are taken up, resulting in small loads generated primarily by frictional contacts between crossover points as the structure trellises. The transition to the second region occurs when adjacent spacing between parallel strands is reduced to zero, and is marked by an exponential ramping in the force vs. displacement curve. This ramping is due to fiber rearrangement and the diminishing of residual gaps between fibers within the strand and the beginning of fiber compaction. Finally, the third region is characterized by abrupt increases in load for small increments of axial displacement and strain, which results from lateral compression of strand fibers in a fully consolidated state.

The desired or novel braid response can be thought of as containing an additional low-load region of deformation, occurring within the stiffening portion of the braid response. This means, an initially stiff behavior displayed under normal conditions, gives way to a

MODELING

This paper addresses braid mechanics based on a geometric foundation. Geometric models assume predetermined geometric responses with respect to external loading conditions [2-4]. Specifically, a combination of two different geometric models is used to predict braid response: kinematic and differential geometry. Braid trellising due to a reduction in adjacent parallel strand spacing is characterized using a purely kinematic idealization and accounts for the zero load region (I) described in Fig.1. The remaining ramping(II) and stiffening(III) regions of braid deformation are modeled using a geometric differential model from Seo [4] modified by experimental strand compaction data.

KINEMATIC MODEL

The kinematic model represents the low or zero load region of shear deformation and is used as an indicator to predict the braid angle at which wrinkling occurs. At this wrinkling point, parallel strands first contact, and strand spacing, d , diminishes to zero for coverage equal to unity. This point in deformation also marks the transition from the kinematic model to the modified differential geometry representation. In the kinematic approach, the braid is considered a planar linkage having a rotational degree of freedom about axes normal to strand intersections [5,6]. The resulting mechanized pin joint construction lends itself to being described very easily through simple geometric principles (Fig. 3).

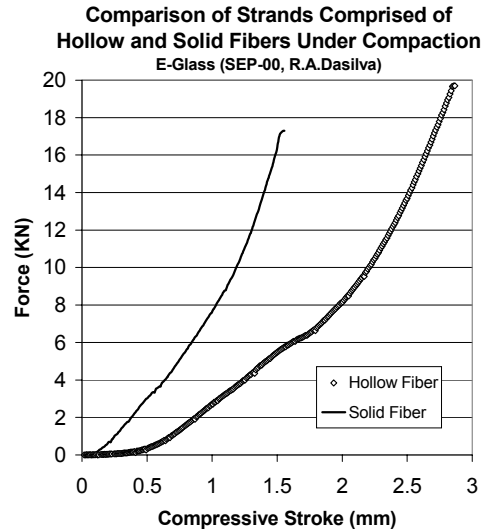
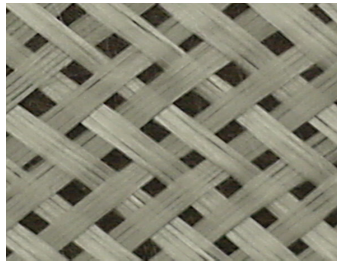
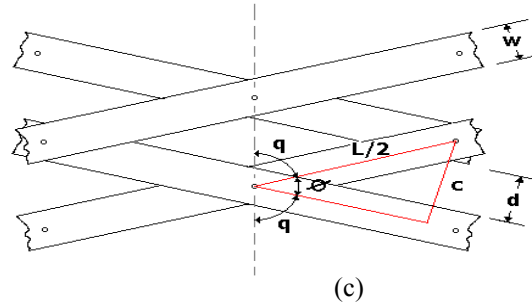


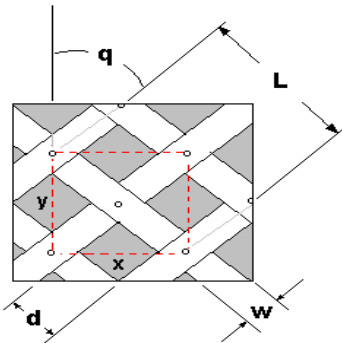
Fig. 2. Comparison of hollow and solid fiber strands under compaction



(a)



(c)



(b)

Fig. 3. Kinematic Model Geometry (a) 2x2 braid; (b) braid schematic; (c) pin-joint geometry

It is assumed that the distance between pins, $L/2$, never changes and thus there is no relative sliding between crossing links. The relationship between the braid angle, q , and the parallel strand spacing, d , is fairly straightforward (Eqn.1). This kinematic model predicts the braid angle (or helix angle) at which the transition between regions I and II of the braid response (Fig. 1) occur.

$$d = \frac{L}{2} \cdot \sin(2 \cdot q) - w \quad (1)$$

STIFFENING MODEL

Axial rope stiffness past the wrinkling point is determined by examining the stiffness of a single strand within the braid. More specifically, a strain or extension in the strand will result in a corresponding load as a function of the axial stiffness of the strand. Transforming the load from the strand direction to the axial rope direction, about the braid angle q , and multiplying that load by the number of strands in the braid, yields a cumulative rope load.

Differential Geometry Formulation

Initial description of the braid geometry is based on a single strand differential geometry method by Seo [4]. In this approach, the path of a single strand is assumed to wrap and ascend about the rope axis to form a helix, with a constant angle, q , for one rotation or cycle of 2π radians, as measured by θ , which is the projection of the primary helix onto the x-y plane (Fig. 4).

Furthermore, through its path, the strand is assumed to undulate about the primary helix in a sinusoidal nature, with an amplitude equal to the thickness of the crossing yarns it intersects. However, the assumption is made that the strand is not crimped at the crossover points, and therefore has a uniform cross-section. The strand position is described using the vector \vec{R}_P , taken from the origin of the Cartesian coordinate system. The vector \vec{R}_H describes the helix position, while the vector \vec{R}_N describes the amplitude of strand undulation projected in the x-y plane. The derivation of Eqn. 2, which describes the length of the strand, can be found in Seo [4].

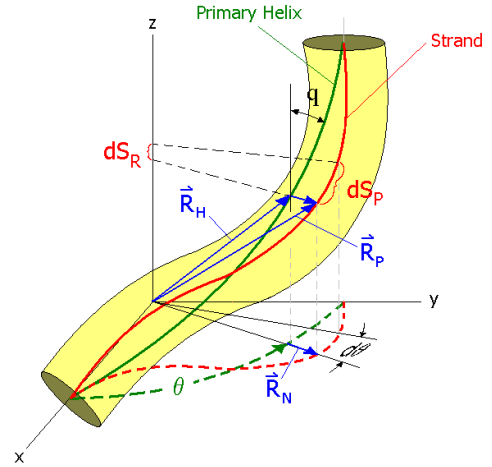


Fig. 4. Differential geometry for quarter cycle.

$$ds_p = \sqrt{A + B \sin(T\theta) + C \sin^2(T\theta)} \cdot d\theta \quad (2a)$$

where

$$A = R_m^2 \cdot [1 + \cot^2 q] + R_N^2 \cdot T^2 \quad (2b)$$

$$B = -2 \cdot R_m \cdot R_N \quad (2c)$$

$$C = R_N^2 \cdot (1 - T^2) \quad (2d)$$

Since Eqn. 2 describes the differential length along the strand at any angle θ , it is necessary to sum all of these differential lengths, or integrate over one full cycle in order to determine the strand length, S .

$$S = \sum_{n=0}^{359} \left(\frac{CR_{n+1} + CR_n}{2} \right) \cdot (\theta_{n+1} - \theta_n) \quad (3)$$

Compaction Modified Mechanical Model

The following section deals with integrating the compaction findings with the existing model structure. To accomplish this task, a new module was created which describes the tensile braid behavior as a function of lateral strand mechanics. The first step in developing the compaction model is to consider the braid as an arrangement of springs. For simplification, consider a braid with the minimum possible number of strands, that being three. Figure 5 illustrates the spring system representation of the braid in tension, where K_{Aeq} and dA are the axial stiffness and elongation of the strand for one helix cycle and K_{Teq} and dT are the transverse strain stiffness and cumulative change in strand width, respectively. The helix or braid angle, q , is shown in Fig. 5, as well as the braid axial load, F .

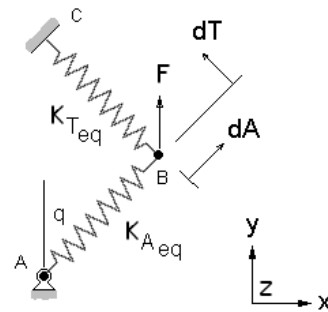


Fig. 5. Equivalent spring system representation

In the physical braid, the K_T series continues around the circumference of the braid, tying into itself, and remains transverse in its orientation to K_A throughout trellising. These equivalent stiffness and deformation terms can be expressed in terms of the individual strand stiffness (k_A and k_T) and the change in width of a single strand (dw). N represents the total number of strands. Note that because they are in parallel, the axial elongation of each strand is the same (dA). The strand stiffness, k_A , can be determined from the strand material and size. The differential model is used as a starting point to calculate the initial strand length, S_p , for determining the value of k_A , which remains a constant in the calculations.

$$K_{Aeq} = \sum_{n=1}^N n \cdot k_A = N \cdot k_A \quad (4)$$

$$K_{Teq} = \frac{1}{\sum_{n=1}^N \frac{n}{k_T}} = \frac{k_T}{N} \quad (5)$$

$$dT = N \cdot dw \quad (6)$$

Figure 6 summarizes how this simple spring model is used in conjunction with experimental lateral compaction data to predict the force vs. displacement response of the braid for regions II and III (Fig.1). Starting from the upper left corner of the flowchart, an increment of transverse strand force, F_T , is specified. The corresponding change in transverse strand width, dw , is obtained from the experimental compaction tests.

$$F_T = k_T \cdot dw = K_{Teq} \cdot dT \quad (7)$$

Equilibrium at point B in Fig. 5 leads to:

$$\sum F_X = -K_{Aeq} \cdot dA \cdot \sin(q) + K_{Teq} \cdot dT \cdot \cos(q) = 0 \quad (8)$$

Solving Eqn. 8 for axial deformation, dA ,

$$dA = \frac{dT \cdot K_{Teq}}{K_{Seq} \cdot \tan(q)} \quad (9)$$

Because of the lateral compaction, dT , the helix angle, q , changes from the initial value. From the geometry shown in Fig. 7, the displacement of the braid, dh , can be expressed as

$$dh = \vec{dr} \cdot \sin(\alpha) \quad (10)$$

where

$$\vec{dr} = \vec{dA} + \vec{dT} \quad (11)$$

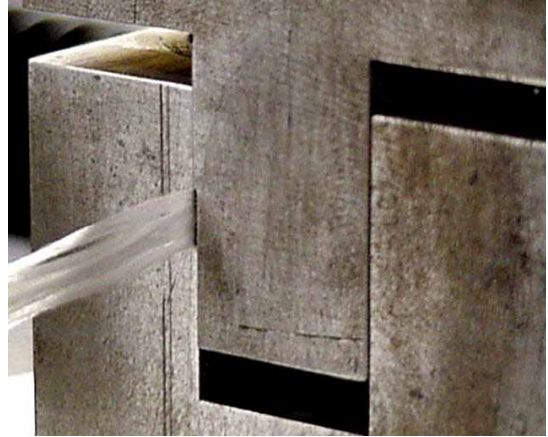


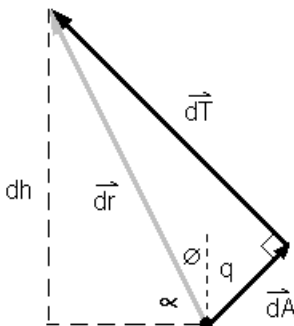
Fig. 8. Strand compaction test fixture

$$\alpha = \frac{\pi}{2} - a \sin\left(\frac{dT}{dr}\right) - q \quad (12)$$

Also, again from equilibrium (Fig. 5), the equation for the force on the braid in the y-direction becomes,

$$F = K_{Aeq} \cdot dA \cdot \cos(q) + F_T \cdot \sin(q) \quad (13)$$

Stran
Latera
8. Str
mating
T-sha
the slc



data

were performed using the yarn compression fixture shown in Fig. 8. Untested braids were inserted on edge into the slot formed by the press (strand width running from top to bottom in the slot). The braid was then plunged into the mating channel, causing a reduction in the cross-section of the strand specimen within.

Fig. 7. Relationship between strand and braid deformation

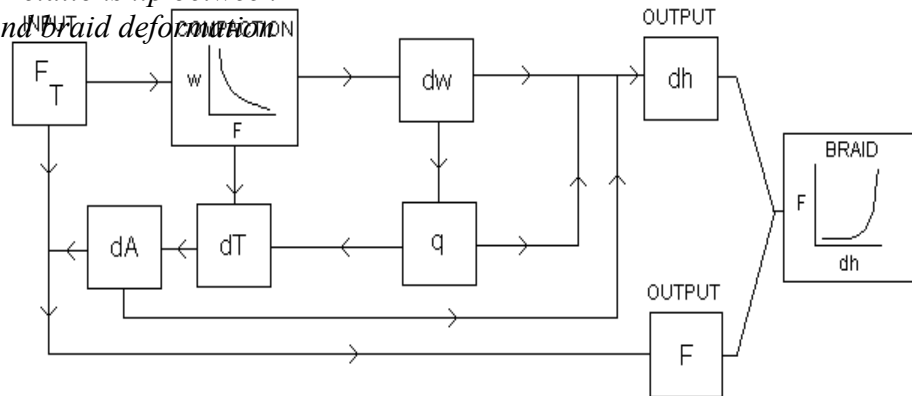


Fig. 6. Flowchart of braid tensile model

To utilize the experimental compaction data in the model, it must be curve fit in terms of some function such that indexing the input value of dw will yield a corresponding value of F_T . Figure 9 gives an example of the curve fitting results for a 12k carbon yarn. To achieve a better fit, the curve was broken up into 3 segments.

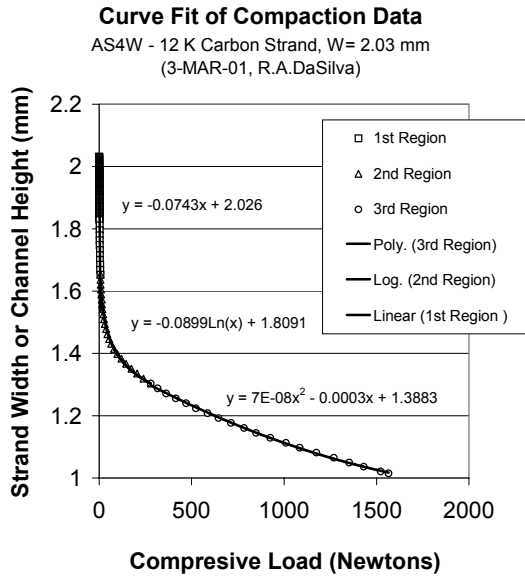


Fig. 9. Curve fit equations for strand lateral compaction

As can be seen in the figure, the curves fit the data well, but do experience some discontinuity at the transition from one function to the next. This is a common occurrence between all of the plots. More importantly, notice that there are three regions of deformation for the strand compaction, similar to the trends seen in the overall braid response. These regions can be categorized as rearrangement, percolation, and consolidation of fibers within the yarn, comparable to that described in particle or powder compaction models [7].

COMPARISON OF MODEL AND BRAID TEST DATA

Force versus displacement curves generated using the equations and methods previously outlined were plotted against data from tension braid tests for Carbon, Nylon, and Glass braids at 30, 45, and 60-degree braid angles. In reviewing the plots, there exists good agreement between theoretical predictions and experimental results. Figure 10 shows the results for a 60-degree

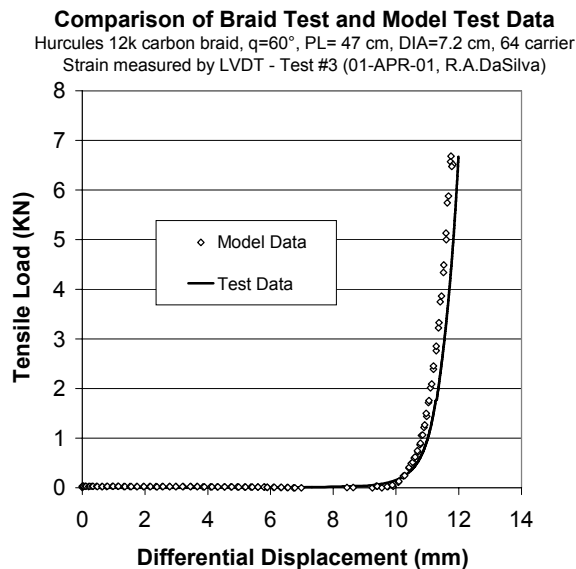


Fig. 10. Comparison of experimental data and model predictions for carbon braid

carbon fiber braid. It represents one of the better agreements between experimental and theoretical data. Note the three regions of deformation and how well they agree in transition with respect to load. Figure 11 presents the results for a nylon braid. The experimental and model results agree well at lower loads; however plastic deformation of the nylon fibers led to a divergence at the higher loads.

Despite the relatively good agreement in these two examples, there were a few substantial causes of disparities between data sets. The first reason lies in the width and shape of the slot machined in the yarn press. That is, a differing slot width or shape will yield a differing mechanical response for the strand, and thus, braid. Since only one glass braid was potted under tension to determine the corresponding slot width for the compaction fixture, there can be no assurance that this is valid for the carbon and nylon compression tests. The major finding of photomicrographs was that the yarn did not change thickness during loading from its manufactured state. However, this may not be the case for all braids and may vary due to angle, material type, length, fiber diameter, number of fibers, etc. To improve the accuracy of results, an adjustable fixture should be designed which allows tailoring to each braid. The second possible reason for error lies in the frictional and pressure effects at the fixture wall – fiber interface. This is more intuitive since in the braid, fibers interface with other fibers from neighboring yarns, and not a steel channel. Thus, sliding behavior of the fibers may not be simulated accurately, yielding less than accurate stiffness response. Third, the bending and crimping in the yarn that occurs in the braid was not accounted for in the model. In actuality, transverse pressures at the yarn interface cause a flattening or crimping of the strand [2]. Additionally, since the strand undulates through the thickness of the braid, it tends to try and straighten out under load, producing a bending mode of deformation in the strand. The last two reasons mentioned, tend to reduce the stiffness of the braid and as with most textile mechanical models, idealizations tend to cause an over prediction of stiffness.

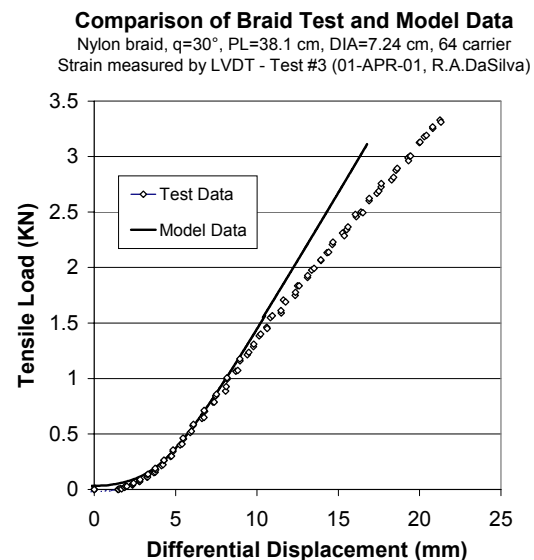


Fig. 11. Comparison of theoretical and experimental data for a nylon braid.

CONCLUSIONS AND FUTURE WORK

It has been argued in the work presented that lateral strand compaction behavior drives overall braid tensile behavior. Arguments are supported by a good correlation between model predictions and experimental tests. It is reasonable to postulate that finding a fiber with a lateral compaction behavior that exhibits the desired plateau will result in an increased toughness in a braid comprised of these novel fibers. This is the most critical finding of the work thus far and has significant meaning in terms of the potential to improve the toughness of current braided structures such as rope and cord. The plateau response can also lead to an extension of the trellising of the braid prior to wrinkling. This can allow for increased deformation in forming of composite parts. However, more tests of braids comprised of these novel yarns need to be conducted to substantiate the theories presented and much work is needed in terms of studying these materials and finding new ones that will produce a more significant magnitude of the same type of novel response.

ACKNOWLEDGMENTS

The authors would like to thank the National Textile Center for support of this research. Additional student contributors include: Darin Lussier, Samuel Chow, and Anuradha Bulusu. Staff contributors include: Glen Bousquet, Dave Rondeau, and Gary Howe.

REFERENCES

- [1] Vallee, D.R, Dion, *M.R.*, *Southern New England Tropical Storms and Hurricanes, A Ninety-eight Year Summary 1909-1997*, National Weather Service, Taunton, MA.
- [2] Ryan, R.J., 1999, *Oceans Conference '99 – IEEE Conference Proceedings*, pp.698 – 701.
- [3] Wu, H-C, Seo, M.H., Backer, S., and Mandell, J.F., 1995, “Structural modeling of double-braided synthetic fiber ropes,” *Textile Research Journal*, v65, n11, p.619.
- [4] Seo, M.H., 1988, “Mechanical deterioration of synthetic fiber rope in marine environment,” *PhD Thesis*, Mech. Eng., M.I.T.
- [5] McBride, T.M. and Chen, J., 1997, “Unit-cell geometry in plain-weave fabrics during shear deformation,” *Comp Sci & Tech*, 57, pp.345-351.
- [6] Prodromou, A.G., and Chen, J., 1997, “On the relationship between shear angle and wrinkling of textile composite performs,” *Composites Part A*, 28A, pp.491-503.
- [7] Santos, C.A.M., Fernandes, R.T., and Strecker, K., 1996, “A Modified Model Describing the Compaction Behaviour of Ceramic and Metal Powders,” *J Materials Science Letters*, 15, pp.1562-1564.

Website URL: <http://m-5.uml.edu/acmtrl/ntc/M98-D03.htm>